Journal of Alloys and Compounds 647 (2015) 265–275

Contents lists available at ScienceDirect

Journal of Alloys and Compounds

journal homepage: http://www.elsevier.com/locate/jalcom

Investigation of structural and optical properties of $CaTiO_3$ powders doped with Mg^{2+} and Eu^{3+} ions

Larissa H. Oliveira [a, *], Julia Savioli [b], Ana P. de Moura [a], Içamira C. Nogueira [b], Maximo S. Li [c], Elson Longo [a], José A. Varela [a], Ieda L.V. Rosa [b]

[a] Institute of Chemistry, State University of São Paulo, 14800-900, Araraquara, São Paulo, Brazil
[b] Department of Chemistry, Federal University of São Carlos, 13565-905, São Carlos, São Paulo, Brazil
[c] Institute of Physics, University of São Paulo, P.O. Box, 13566-590, São Carlos, São Paulo, Brazil

ARTICLE INFO

Article history:
Received 20 January 2015
Received in revised form
18 May 2015
Accepted 19 May 2015
Available online 14 June 2015

Keywords:
A. Ceramics
B. Chemical synthesis
C. Optical properties
C. Order-disorder effects

ABSTRACT

In this work, $CaTiO_3$ powders doped with Mg^{2+} ions and $CaTiO_3$ powders co-doped with Mg^{2+} and Eu^{3+} ions were prepared by the polymeric precursor method (PPM). These powders were characterized by different characterization techniques to study the influence of Mg^{2+} doping as well as Mg^{2+} and Eu^{3+} co-doping in structural and optical properties of $CaTiO_3$ perovskite-type structure. The Rietveld refinement and Micro-Raman analyses suggested the substitution Mg^{2+} and Eu^{3+} ions in the A-site of $CaTiO_3$ perovskite. The influence of Mg^{2+} doping can be detected by the displacement of calcium and oxygen atomic positions when compared to the non-doped $CaTiO_3$ powder. When Eu^{3+} ions are added to the A-site of this perovskite the excess of positive charge can be compensated by the formation of calcium vacancies. Luminescence data showed that $Ca_{1-x}Mg_xTiO_3$ and $Ca_{1x}Mg_{x/2}Eu_{2y/3}TiO_3$ powders are potential materials for fabrication of lighting devices based on near-UV and blue LED using an excitation wavelength of 397 and/or 450 nm.

1. Introduction

$CaTiO_3$ belong to the perovskite class materials (ABO_3) and it is also a chemistry and thermally stable ceramic oxide, which is widely studied due to its dielectric and photoluminescent properties [1,2]. $CaTiO_3$ has an orthorhombic structure and space group *Pbnm* which remains stable from 23 to 1100 °C [3] and it has a dielectric permittivity of approximately 180 at room temperature that changes with experimental conditions. This ceramic oxide is also a good candidate to be applied in electronic microwave devices due to its high quality factor (Qu = 8000 at 1.5 GHz) specially when in solid solution with $Sr(Mg_{1/3}Nb_{2/3})O_3$(SMN) (Qu = 20000 at 1.5 GHz) or $MgTiO_3$ (Qu = 8000 at 7.5 GHz) materials. The $CaTiO_3$ based solid solution such as $CaTiO_3$–$LaAlO_3$ can also be applied as high performance capacitors [4–6].

Among to these systems, we highlighted the $CaTiO_3$–$MgTiO_3$, which presents outstanding dielectric properties allowing its application in resonators dielectric devices, filters and antennas operating in microwave range frequency [7]. Moreover, the dielectric properties such as dielectric permittivity (k), quality factor (Q × f) and stabilization temperature (τ_f) are tunable by $CaTiO_3/MgTiO_3$ ratio in this solid solution and depends on the partial pressure of O_2 used during the sintering procedure [8]. In order to use them in miniaturized electronic devices, these systems have also been synthesized as thin films and multilayer heterojunctions. In another study, the dependency of composition heterogeneity and dielectric properties of $Mg_{0,93}Ca_{0,07}TiO_3$–$Ca_{0,30}Li_{0,14}Sm_{0,42}TiO_3$ heterostructure was investigated [9].

$CaTiO_3$ and $MgTiO_3$ matrixes exhibited a photoluminescence emission in the visible region of the electromagnetic spectrum. These findings of perovskites-type structures have reactivated the investigation of their luminescent mechanisms due to continuous request for new phosphor materials as compact light sources and photonic devices to obtain short wavelength sources that can be pumped with diode lasers [10]. $CaTiO_3$ doped with rare earth (RE) ions [12–15] presents various applications in the fields of optoelectronic devices and have attracted a lot of attention because of their promising luminescent properties, friendly environment and well-known chemical stability for being applied in field emission

* Corresponding author.
E-mail address: larissahelena2009@gmail.com (L.H. Oliveira).

http://dx.doi.org/10.1016/j.jallcom.2015.05.226
0925-8388/

displays and white-light emitting diodes (wLEDS) devices [15].

In order to enhance the luminescent properties many researchers have concentrated on varying the concentration of RE ions as well as charges compensators like Al^{3+}, In^{3+}, Ga^{3+}, Mg^{2+}, Zn^{2+} and Li^{+} ions. In $CaTiO_3$:Pr^{3+} doped Li^{+} thin films [16], Li^{+} ions increased the emission quantum efficiency and also promoted some changes in the morphology as well as particles grain size. Gasparotto et al. [17] studied the photoluminescent properties of $LiTaO_3$ powders co-doped with Eu^{3+} and Mg^{2+} prepared by the polymeric precursor method. The presence of Mg^{2+} also increased the luminescence intensity of the emission bands due to local lattice distortion effects as well as luminescence mechanisms associated to the energy transfer from the host lattice to RE^{3+} ions. The same effect was observed in RE doped alkaline-earth stannates such as Tb–Mg–$SrSnO_3$, where an intense white luminescence was observed. Due to capacity of these systems to amplify light, they can be potential candidates for application in integrated optoelectronic devices [18].

Based on the potential application of $CaTiO_3$-doped systems, we investigated the influence of Mg^{2+} doping as well as Mg^{2+} and Eu^{3+} co-doping in the crystalline structure of $CaTiO_3$ matrix. In this work, $Ca_{1-x}Mg_xTiO_3$ powders with $x = 0.0$, 0.005, 0.01 and 0.02 mol of Mg^{2+} ions and $Ca_{1-x}Mg_{x/2}Eu_{2y/3}TiO_3$ powders with $x = 0.000$, 0.001, 0.002, 0.003 and 0.004 mol of Mg^{2+} and Eu^{3+} ions were prepared by PPM [19] and characterized by X-Ray diffraction (XRD), micro-Raman spectroscopy (MR) and Ultraviolet–visible (UV–vis) absorbance spectroscopy. The photoluminescent properties (PL) were studied by emission spectra with excitation centered in the host lattice. However, the PL properties of $Ca_{1-x}Mg_{x/2}Eu_{2y/3}TiO_3$ matrices were investigated by emission and excitation spectra of the Eu^{3+} ion. The lifetimes of the Eu^{3+} $^5D_0 \rightarrow {}^7F_2$ transition ($\lambda_{exc} = 397$, $\lambda_{em} = 617$ nm) were also evaluated.

2. Experimental procedure

2.1. Preparation of the titanium citrate solution

Titanium citrate solution was prepared by adding an amount of citric acid in 1 L of deionized water at 60 °C. Obeying a titanium/citric acid molar ratio of 1:3, 40 mL of titanium isopropoxide ($[Ti(OC_3H_7)_4]$) was also added to the above solution. The resulting mixture remained under constant stirring and heating until its complete homogenization. After filter, this citrate solution was subjected to a gravimetric analysis, where a concentration of 1.4 mmol/g of TiO_2 was obtained.

2.2. Preparation of $Ca_{1-x}Mg_xTiO_3$ and $Ca_{1-x}Mg_{x/2}Eu_{2y/3}TiO_3$ powders

$Ca_{1-x}Mg_xTiO_3$ powders were prepared following the experimental procedure described below: In a Becker vessel containing 10 mmol of titanium citrate at 60 °C, $1 - x$ mol of $Ca(NO_3)_2{\cdot}4H_2O$ was added under constant stirring. After complete dissolution, stoichiometric quantities of $x = 0.00$; 0.005; 0.01 and 0.02 mol of $Mg(NO_3)_2.6H_2O$ were also added to this system.

For $Ca_{1-x}Mg_{x/2}Eu_{2y/3}TiO_3$ powders charge and mass balance was performed [20]. The necessary amounts of europium (z) and magnesium (y) are equal when charge balance is considered ($3z = 2y$) and when mass balance is considered totalize an amount of $x = 0.000$, 0.001, 0.002, 0.003 and 0.004 mol of Mg^{2+} and Eu^{3+} ions ($3z + 2y = x$). Thus, $1 - x$ mol of $Ca(NO_3)_2{\cdot}4H_2O$, $y = x - 3z/2$ mol of $Mg(NO_3)_2{\cdot}6H_2O$ and $z - 2y/3$ mol of $Eu(NO_3)_3{\cdot}xH_2O$ was added to the titanium citrate solution.

The temperature was raised to 90 °C and ethylene glycol was added to the reactional mixture using a mass ratio (citric acid/ethylene glycol) of 40:60. The solvent (water) was evaporated resulting in a polymeric resin. The polymeric resin was dried in a conventional oven at 350 °C for 8 h. Then, the resulting powder was annealed in a tubular oven at 800 °C for 8 h using a heating rate of 10 °C/min under O_2 flux.

2.3. Characterizations

The as-prepared powders were structurally characterized by XRD in a Rietveld routine using a Rigaku-DMax/2500PC (Japan) with Cu-Kα radiation ($\lambda = 1.5406$ Å) and in the 2θ range from 10° to 130° with a scanning rate of 0.02°/min. MR spectra were collected using a 514.5 nm line of a Ar laser (output 8 mM) in a Jobin-Yvon model T64000 spectrometer. Uv–vis absorption spectra were performed using Cary 5G equipment. PL measurements were performed in a 139 Thermal Jarrel-Ash Monospec 27 monochromator and a Hamamatsu R446 photomultiplier. The 350 nm exciting wavelength of a krypton ion laser (Coherent Innova) was used keeping a nominal output power of 200 mW. Photoluminescence properties of $Ca_{1-x}Mg_{x/2}Eu_{2y/3}TiO_3$ powders were investigated monitoring the *f–f* intraconfigurational transitions of Eu^{3+} ions. Excitation and emission spectra were collected in a Jobin Yvon-Fluorolog (model #FL3-222) spectrofluorometer using a Xenon lamp (ozone free) as excitation source. Lifetime data of the Eu^{3+} $^5D_0 \rightarrow {}^7F_2$ transition were collected using a Jobin Yvon phosphorimeter (model # FL 1040). For decay curves acquisition was used the emission wavelength set at 617 nm and excitation wavelength set at 397 nm. All the measurements were performed at room temperature.

3. Results and discussion

3.1. X-ray diffraction (XRD) and structural refinement Rietveld analysis

In this work, we synthesize $Ca_{1-x}Mg_xTiO_3$ powders with $x = 0.0$; 0.005; 0.01 and 0.02 mol of Mg^{2+} ions to analyze the influence of Mg^{2+} doping in the crystalline structure of $CaTiO_3$ matrix. The co-doping effect of Mg^{2+} and Eu^{3+} ions were also analyzed in$Ca_{1-x}Mg_{x/2}Eu_{2y/3}TiO_3$ powders with $x = 0.000$, 0.001, 0.002, 0.003 and 0.004 mol of Mg^{2+} and Eu^{3+} ions. Fig. 1 (a) and (b) presents the XRD patterns of $Ca_{1-x}Mg_xTiO_3$ and $Ca_{1-x}Mg_{x/2}Eu_{2y/3}TiO_3$ powders prepared by the PPM, respectively. As it can be seen, these powders crystallized in a $CaTiO_3$ orthorhombic phase and space group *Pbnm*, in accordance to the Inorganic Crystal Structure Database (ICSD) card number 74-212. $Ca_{1-x}Mg_xTiO_3$ powders with $x = 0.005$ and 0.01, presented a rutile TiO_2 secondary phase with a tetragonal structure and space group *P42/mnm* according to the ICSD card number 36-212 (●). On the other hand, $Ca_{1-x}Mg_xTiO_3$ composition with $x = 0.02$ presented a trigonal $MgTiO_3$ secondary phase with space group *R-3H* as observed, according to the ICSD card number 55-285 (◆), probably indicating that the solubility limit of Mg^{2+} ions in the $CaTiO_3$ matrix was achieved in the range of 0.01 and 0.02% of Mg^{2+} ions. None secondary phases were detected in the $Ca_{1-x}Mg_{x/2}Eu_{2y/3}TiO_3$ powders indicating that both Eu^{3+} and Mg^{2+} ions were incorporated to the $CaTiO_3$ matrix.

The average of crystallite sizes were estimated by Scherrer's equation using the full width at half maximum (FWHM) of the most intense peak at 2θ ~33.2. As reported in the literature [21], the Scherrer equation (1) is described as follows:

$$D = \frac{0.9\lambda}{B\cos\theta} \quad (1)$$

D is the average crystallite size, λ the X-ray wavelength (0.15406 nm), θ the Bragg angle and B is the FWHM. The values of

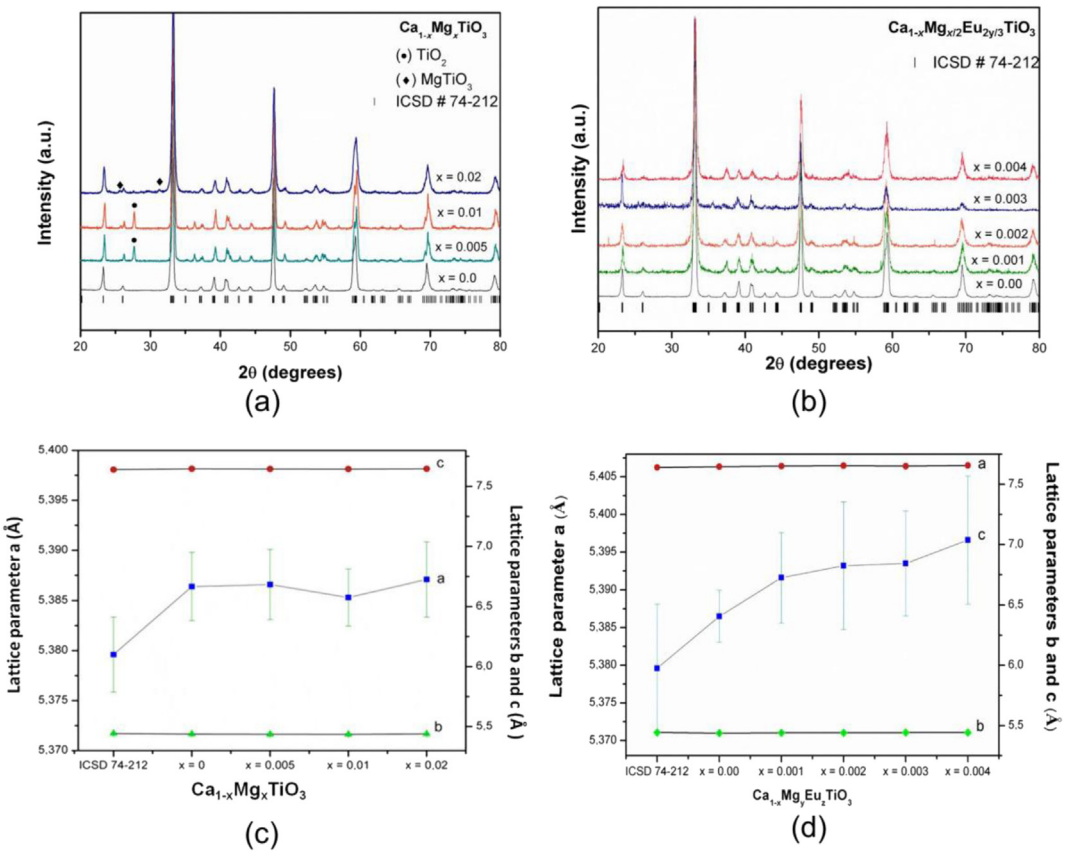

Fig. 1. XRD patterns of $Ca_{1-x}Mg_xTiO_3$ powders with $x = 0.000$, 0.005, 0.01 and 0.02 mol of Mg^{2+} ions (a) XRD patterns of the $Ca_{1x}Mg_{x/2}Eu_{2y/3}TiO_3$ powders with $x = 0.000$, 0.001, 0.002, 0.003 and 0.004 mol of Mg^{2+} and Eu^{3+} ions (b), lattice parameters a, b and c of $CaTiO_3$ matrix as function of Mg^{2+} doping (c) and lattice parameters a, b and c of CaTiO3 matrix as function of Mg^{2+} and Eu^{3+} co-doping (d), respectively.

crystallite size of $Ca_{1-x}Mg_xTiO_3$ and $Ca_{1-x}Mg_{x/2}Eu_{2y/3}TiO_3$ powders are presented at Tables 1 and 2, respectively. As can be seen, the Mg^{2+} doping and Mg^{2+} and Eu^{3+} co-doping promoted a decrease in crystallite size. This behavior can be associated to the replacement of Ca sites into the perovskite structure by the Mg and Mg and Eu atoms in these systems. Thus, Rietveld analyses were employed in order to estimate the influence of the doping on the lattice parameters of $Ca_{1-x}Mg_xTiO_3$ and $Ca_{1-x}Mg_{x/2}Eu_{2y/3}TiO_3$ powders.

Rietveld measurement was performed through the GSAS (General Structure Analysis System) program [22]. The background was corrected using a Chebyschev polynomial of the first kind. The diffraction peak profiles were better fitted by Thompson–Cox–Hastings pseudo-Voigt (pV-TCH) function and by asymmetry function described by Finger et al. [23].

The lattice parameters (a, b and c), unit cell volume (V), rotation angle (α) between adjacent [TiO_6] clusters and the correlation parameters (R_{wp}, R_{Bragg}, χ^2) of both $Ca_{1-x}Mg_xTiO_3$ and $Ca_{1-x}Mg_{x/2}Eu_{2y/3}TiO_3$ powders are listed at Tables 1 and 2, respectively. The Rietveld data show a good relation between the observed XRD patterns and the theoretical ones. The quantative analysis of phases showed that the calculated percentage of TiO_2phase in $Ca_{1-x}Mg_xTiO_3$ powders with $x = 0.005$ and 0.01 was 7.06% and 6.52%, respectively. Moreover, the percentage of $MgTiO_3$ phase in $Ca_{1-x}Mg_xTiO_3$ powders with $x = 0.02$ was 0.91%.

These results demonstrated that Mg^{2+} doping has a strong influence on the crystallinity of the host structure, hence, the lattice parameter increases as a function of the Mg^{2+} ions concentration. This behavior was associated to the difference of ionic radii between the Ca^{2+} and Mg^{2+} ions as well as repulsions caused by the replacement of Ca^{2+} by Mg^{2+} ions in the A site of the perovskite structure, since both presents a ionic character with radial orientation. This effect changes the chemical environment of $CaTiO_3$ matrix, resulting in a TiO_2 secondary phase. Besides that, when the solubility limit is reached, it was observed the formation of $MgTiO_3$ instead of TiO_2 phase. These results are in accordance to the crystalline size values obtained by Scherrer's equation.

Table 1
Lattice parameters (a, b and c), rotation angle (α) between adjacent [TiO_6] clusters, unit cell volume (V), crystallite size and correlation parameters (R_{wp}, R_{Bragg} and χ^2) of $Ca_{1-x}Mg_xTiO_3$ systems obtained by Rietveld refinement method.

$Ca_{1-x}Mg_xTiO_3$	a (Å)	b (Å)	c (Å)	α	V (Å^3)	Crystallite size (nm)	R_{wp} (%)	R_{Bragg} (%)	χ^2
ICSD# 74-212	5.3796	5.4426	7.6401	156.8°	223.7	–	–	–	–
x = 0.0000	5.3865 (8)	5.4374 (8)	7.6464 (11)	156.3°	223.9 (80)	59.64	8.44	3.14	1.31
x = 0.005	5.3864 (21)	5.4349 (20)	7.6444 (34)	156.8°	223.8 (14)	46.12	23.25	8.63	1.30
x = 0.01	5.3842 (30)	5.4335 (25)	7.6420 (4)	155.5°	223.6 (14)	43.69	24.13	7.70	1.36
x = 0.02	5.3871 (13)	5.4387 (14)	7.6467 (20)	156.5°	224.0	38.62	8.3	3.28	1.21

Table 2
Lattice parameters (a, b and c), rotation angle (α) between adjacent [TiO_6] clusters, unit cell volume (V), crystallite size, Mg/Eu ratio and correlation parameters (R_{wp}, R_{Bragg} and χ^2) of $Ca_{1x}Mg_{x/2}Eu_{2y/3}TiO_3$ systems obtained by Rietveld refinement method.

$Ca_{1-x}Mg_{x/2}Eu_{2y/3}TiO_3$	a(Å)	b(Å)	c(Å)	α	V(Å^3)	Mg/Eu	Crystallite size (nm)	R_{wp} (%)	R_{Bragg} (%)	χ^2
ICSD# 74-212	5.3796	5.4426	7.6401	156.8°	223.7	–	–	–	–	–
x = 0.0000	5.3865 (8)	5.4374 (8)	7.6464 (11)	156.3°	223.9 (80)	0.0	59.64	8.44	3.14	1.31
x = 0.0001	5.3916 (12)	5.4395 (6)	7.6509 (11)	157.9°	224.7 (90)	2.2	49.88	9.65	8.43	1.37
x = 0.0002	5.3932 (14)	5.4398 (31)	7.6551 (15)	156.54°	224.6 (90)	2.1	40.26	10.29	7.16	1.43
x = 0.0003	5.3935 (14)	5.4414 (12)	7.6504 (10)	157.21°	224.5 (80)	2.2	113.08	12.35	7.08	1.11
x = 0.0004	5.3966 (17)	5.4417 (9)	7.6562 (17)	153.95°	224.8 (80)	1.5	42.12	12.98	9.38	1.29

Unlike the Mg^{2+} doping, Table 2 demonstrates that Mg^{2+} and Eu^{3+} do not affect significantly the crystalline structure of host matrix. The slight differences in the c lattice parameter observed for $Ca_{1-x}Mg_{x/2}Eu_{2y/3}TiO_3$ powders (Fig. 1(d)), probably indicates that both ions are capable of replace the Ca^{2+} ions in $CaTiO_3$ matrix acting as a luminescence centers [24]. This is only possible due to a small difference in ionic radii of Eu^{3+} (94.7 pm) and Mg^{2+} (57 pm) together when compared to Ca^{2+} ions (100 pm), in coordination number of 6 [25]. Moreover, $Ca_{1-x}Mg_{x/2}Eu_{2y/3}TiO_3$ system with $x = 0.004$ presented the highest lattice parameter and unit cell volume values, probably indicating the formation of a solid solution. The same behavior was verified in $Sr_{1+x}Sm_{1-x}Al_{1-x}Ti_xO_4$ systems prepared by the solid state reaction [24]. These results are also in accordance to the crystallite sizes obtained for these systems.

From Rietveld data, the influence of Mg^{2+} doping into $CaTiO_3$ can be noticed by atomic displacements in the Ca, Ti, O atomic positions (x, y and z) when compared to the non-doped $CaTiO_3$ (Table 3). Moreover, the highest changing was observed for calcium and oxygen (O1) positions, indicating that magnesium atoms probably promoted distortions along the Ca–O linkages. The ideal $CaTiO_3$ perovskite structure with space group *Pbnm*, presents the titanium atoms, as lattice formers, in an octahedral coordination to oxygen atoms ([TiO_6]), while calcium atoms as lattice modifiers, in a twelve-fold coordination to oxygen atoms ([CaO_{12}]). As there is the interconnection of [MgO_{12}] and [CaO_{12}] clusters in the perovskite structure, it was possible to conclude that the distortions along [CaO_{12}] clusters caused by the [MgO_{12}] ones can promote the deformation of the Ca–O bonds. This phenomenon is more evident when a second dopant (Eu^{3+} ions) are added in the A site of $CaTiO_3$ perovskite, where more evident displacement in the calcium (Ca) and oxygen (O1) positions is observed (Table 4). Therefore, we can attribute this behavior the increase in the number of distorted [CaO_{12}] clusters into the $CaTiO_3$ orthorhombic structure.

Table 4
Lifetime values (τ) of $Ca_{1-x}Mg_yEu_zTiO_3$ powders with $x = 0.001, 0.002, 0.003$ and 0.004 mol of Mg^{2+} and Eu^{3+} ions obtained from decay curves ($\lambda_{exc} = 397$ nm; $\lambda_{em} = 617$ nm).

$Ca_{1-x}Mg_{x/2}Eu_{2y/3}TiO_3$	τ (ms)
$x = 0.001$	0.94
$x = 0.002$	0.89
$x = 0.003$	1.06
$x = 0.004$	1.01

Mg^{2+} doping and of Mg^{2+} and Eu^{3+} co-doping has a strong influence in the crystalline structure of $CaTiO_3$. In both cases, major changes in lattice parameters and atomic positions are related to the Ca atoms, suggesting that substitution of the A site of perovskite lead to distortions and strains in the host lattice. Thus, MR spectroscopy can be used in order to determine the degree of structural defects or asymmetric–symmetric into the $CaTiO_3$ lattice.

3.2. Micro-Raman (MR) spectroscopy analysis

Fig. 2 presents the MR spectra of $Ca_{1-x}Mg_xTiO_3$ powders with $x = 0.0$; 0.005; 0.01 and 0.02 mol of Mg^{2+} ions and $Ca_{1-x}Mg_{x/2}Eu_{2y/3}TiO_3$ powders with $x = 0.000$, 0.001, 0.002, 0.003, 0.004 mol of

Table 3
Positions of Ca, Ti and O atoms (x, y and z) obtained by Rietveld refinement method for $Ca_{1-x}Mg_xTiO_3$ and $Ca_{1x}Mg_{x/2}Eu_{2y/3}TiO_3$ powders.

Atoms	$Ca_{1-x}Mg_xTiO_3$			
	$x = 0.000$	$x = 0.005$	$x = 0.01$	$x = 0.02$
Ca (x,y,z)	0.9929 (30), 0.03366 (14), 0.25	0.9933 (40), 0.03452 (10), 0.25	0.9901 (28) 0.03515 (15), 0.25	0.9930 (30), 0.03438 (7), 0.25
Ti (x,y,z)	0, 0.5, 0	0, 0.5, 0	0, 0.5, 0	0, 0.5, 0
O1 (x,y,z)	0.0724 (6), 0.484 (14), 0.25	0.07139 (10), 0.4821 (20), 0.25	0.076 (4), 0.4856 (16), 0.25	0.07151 (9) 0.4823 (17), 0.25
O2 (x,y,z)	0.7119 (4), 0.2870 (4), 0.03639 (25)	0.7134 (2), 0.2901 (3) 0.03715 (8)	0.7097 (3), 0.2924 (6) 0.0341 (23)	0.7122 (3), 0.2871 (1) 0.0376 (9)

Atoms	$Ca_{1-x}Mg_{x/2}Eu_{2y/3}TiO_3$				
	$x = 0.000$	$x = 0.001$	$x = 0.002$	$x = 0.003$	$x = 0.004$
Ca (x, y, z)	0.9929 (30), 0.03366 (14), 0.25	0.9924 (9), 0.0320 (4), 0.25	0.9971 (11), 0.03068 (31), 0.25	0.9899, 0.02889, 0.25	0.9947, 0.02973, 0.25
Ti (x,y,z)	0, 0.5, 0	0, 0.5, 0	0, 0.5, 0	0, 0.5, 0	0, 0.5, 0
O1(x,y,z)	0.0724 (6), 0.484 (14), 0.25	0.0665 (16), 0.4813 (15), 0.25	0.0710 (14), 0.04805 (12), 0.25	0.0714, 0.4983, 0.25	0.0815, 0.4965, 0.25
O2(x,y,z)	0.7119 (4), 0.2870 (4), 0.03639 (25)	0.7026 (10), 0.2834 (12), 0.0351 (7)	0.7079 (8), 0.2837 (10), 0.0354 (5)	0.7117 (17), 0.2805 (16), 0.0376 (9)	0.7130 (15), 0.2862 (13), 0.0366 (8)

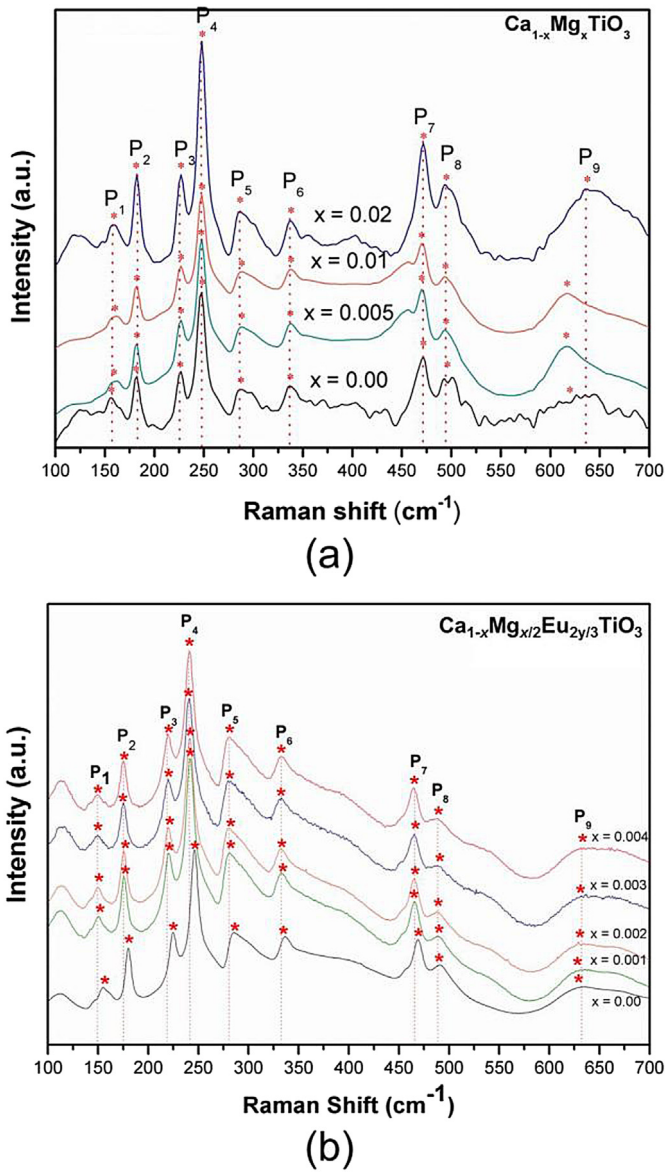

Fig. 2. MR spectra of $Ca_{1-x}Mg_xTiO_3$ (a) and $Ca_{1x}Mg_{x/2}Eu_{2y/3}TiO_3$ (b) powders prepared by the polymeric precursor method.

Mg^{2+} and Eu^{3+} ions in the range of 100 and 700 cm^{-1}.

Literature reports 24 Raman active modes for orthorhombic $CaTiO_3$ perovskite structure and space group *Pbnm* with four clusters per unit cell (Z = 4), represented by equation (2) below [26]:

$$\Gamma_{(\text{Raman})} = 7A_g + 7\,B_{1g} + 5\,B_{2g} + 5B_{3g} \quad (2)$$

For $CaTiO_3$ powder prepared by PPM only nine Raman active modes (P_1, P_2, P_3, P_4, P_5, P_6, P_7, P_8 and P_9) was observed in Fig. 2. P_1 Raman mode (at 156 cm^{-1}) is attributed to the vibration mode of the Ca–TiO_3 orthorhombic structure, while the P_2 (182 cm^{-1}) P_3 (225 cm^{-1}) P_4 (247 cm^{-1}), P_5 (287 cm^{-1}) and P_6 (336 cm^{-1}) Raman modes are related to the bending of the O–Ti–O linkages, caused by the "*tilt*" phenomenon between the *TiO_6-α-TiO_6* adjacent clusters. P_7 (472 cm^{-1}) and P_8 (493 cm^{-1}) Raman modes are attributed to torsions modes of Ti–O linkages, while P_9 (631 cm^{-1}) is related to the vibration asymmetric stretching of these bonds [27–30].

For $Ca_{1-x}Mg_xTiO_3$ powders (Fig. 2(a)), P_1 and P_9 Raman modes are shifted to lower wavenumbers as a function of Mg^{2+} concentration, indicating a probable presence of structural defects and strains into $CaTiO_3$ matrix, which is able to modify the stretching, torsional and bending vibrations of the metal-oxygen bonds. The displacement observed for P_1 Raman mode might be ascribed to distortions along [CaO_{12}] clusters after the introduction of Mg^{2+} ion in these systems. This affect indicates a probable occupancy of the A site (Ca^{2+} ions) position by these ions in the $CaTiO_3$ crystalline structure. Moreover, such distortions modify the electronic density of the [TiO_6] clusters as well as its dipole moment. As a consequence, P_9 Raman mode is also shifted from its usual position [30,31]. From the extended X-ray absorption fine structure (EXAFS) data, Hanajiri et al. [32] also show that doping ions (Ce^{3+} and Nd^{3+}) content can also modifies the Ti–O distances in $CaTiO_3$ matrix.

$Ca_{1-x}Mg_{x/2}Eu_{2y/3}TiO_3$ powders present Raman active modes at 149 (P_1), 175 (P_2) 224 (P_3), 246 (P_4), 285 (P_5), 469 (P_7), 489 (P_8) and 629 (P_9) cm^{-1}, respectively. From Fig. 2 (b), significant differences were observed for P_1 Raman mode. As described above, this behavior can be associated to the presence of dopants (Eu^{3+} and Mg^{2+} ions) in the A site of $CaTiO_3$ matrix. Moreover, this effect enhances the distortion degree of [CaO_{12}] and [TiO_6] clusters in the lattice, shifting the P_2, P_3, P_4, P_5, P_6 modes to lower wavenumbers (Fig. 2(b)). MR data showed that disorder degree at short range along the Ti–O linkages might be due to the symmetry break of [CaO_{12}] clusters caused by structural defects.

The structure and chemistry of this perovskite is associated to distortion from the ideal structure, inducing redistribution on state of densities along the $CaTiO_3$ unit cell. There are several types of lattice defects that are associated with this redistribution.

From X-ray absorption spectroscopy technique (XAS), Milanez et al. [33] indentified two types of charged Titanium complex clusters in $CaTiO_3$ matrix; the [TiO_5 V_O^Z] and [TiO_6] clusters randomly distributed into its crystalline structure. Moreover, [TiO_5 V_O^Z] were associated to oxygen vacancies ($V_O^Z = V_O^X$, $V_O{\bullet}e\,V_O{\bullet\bullet}$), where the double-ionized oxygen vancies ($V_O{\bullet\bullet}$ species) who mainly participates from the conduction mechanism. The charge density is strong influenced by interaction between [TiO_5 V_O^Z] – [TiO_6] clusters. However, Lazaro et al. [34] showed that charge density into $CaTiO_3$ matrix is not only affected by the structural disorder in the network former, but also by structural disorder in the network modifier, thus, this phenomenon was associated to the presence of [CaO_{11} V_O^Z] and [CaO_{12}] complex clusters in the A-site of this perovskite.

For $CaTiO_3$ powders prepared by microwave assisted hydrothermal method, Moreira et al. [35] observed that the distortion degree of (α) angle between [TiO_6] complex clusters is influenced by experimental conditions. Oliveira et al. [31], also showed that distortion degree can also affected by doping elements, such as Cu^{2+} ions, in the A-site of $CaTiO_3$ matrix.

Recently, these structural defects were associated to the nature of lattice formers and modifiers, doping elements, experimental conditions and so on. Other phenomenon can be observed when $CaTiO_3$ matrix is doped with rare earth elements such as Eu^{3+} or Pr^{3+} ions. The substitution of Ca^{2+} by Eu^{3+} ions is responsible by accumulation of positive charge in host matrix. These structural defects may hamper the process of energy transfer from host matrix to rare earth ions [27]. In principle [38], if two Eu^{3+} ions occupy two Ca^{2+} sites, it will generate one Ca^{2+} vacancies, according to charge compensation. The more Eu^{3+} ions were doped into $CaTiO_3$ matrix, more Ca^{2+} vacancy is offered.

The same behavior was verified for Pr^{3+}-doped $CaTiO_3$ powders [37], which it was associated to Ti^{3+} defects as well as oxygen vacancies in the crystalline structure. A part of Pr^{3+} red emission can be reabsorbed in the broad d → d absorption band of Ti^{3+} ions. The oxygen vacancies species are neutral and ionized centers,

contributing to the conduction mechanism in the matrix. The captured electrons in conduction band contributes to non-radiative processes, competing with the energy transfer from matrix to the excited levels of Pr^{3+} ions, corroborating to a decrease in the intensity of the 4f→4f emission. The excess of positive charge can be compensated by intertitals defects, when Ti^{4+} sites are substituted by Al^{3+} ions, improving its optical properties. Mazzo et al. [39] also noticed an improvement in local order-disorder degree by creation of cations or oxygen vacancies with substitution of Eu^{3+} ions in both A and B sites of $CaTiO_3$ matrix. This factor also provided significant changes in local order-disorder degree around Ca and Ti clusters.

Based on these papers, we believe that symmetry break along $[TiO_6]$ and $[CaO_{12}]$ clusters is mainly caused by disorder into the lattice modifiers (Ca atoms) due to distorted $[CaO_{12}]$ clusters and/or Ca^{2+} vacancies in $Ca_{1-x}Mg_xTiO_3$ and $Ca_{1-x}Mg_{x/2}Eu_{2y/3}TiO_3$ powders. These species are strongly related to the formation of $[CaO_{12}]^{\bullet}_{d} \leftrightarrow [CaO_{12}]'_{o}$ clusters (o = ordered, d = disordered) and $V^{z}_{Ca} = V^{x}_{Ca} + V^{\bullet}_{Ca} + V^{\bullet\bullet}_{Ca}$ species in $CaTiO_3$ matrix, respectively. These species are neutral and ionized centers, creating electron–hole pairs (hole (h•)–electron (e^-)-polarons) in the $Ca_{1-x}Mg_xTiO_3$ and $Ca_{1-x}Mg_{x/2}Eu_{2y/3}TiO_3$ powders, contributing to the conduction mechanism in the matrix [35].

3.3. UV–vis absorbance spectroscopy

In this work, the band gap energy (E_{gap}) of the $Ca_{1-x}Mg_xTiO_3$ with $x = 0.00$, 0.005, 0.01 and 0.02 of Mg^{2+} and $Ca_{1-x}Mg_yEu_zTiO_3$ powders with $x = 0.000$, 0.001, 0.002, 0.003 and 0.004 were measured by Kubelka-Munk method [40]. The band gap energy is associated to the electronic transitions, which occurs from the located states in the conduction band (CB) to the located states in the valence band (VB). A direct band gap is related to the electronic transitions that occur from localized states in the same Brillouin region [35], while the indirect band gap is associated to localized states in a different Brillouin region. The band gap (E_{gap}) and the absorption coefficient (α) of a semiconductor oxide are associated according to the equation (3):

$$\alpha h\nu = C_1\left(R_{\infty}(h\nu - E_{gap})^n\right) \quad (3)$$

where α is the linear absorption coefficient of the material, $h\nu$ is the photon energy, C_1 is a proportional constant, E_{gap} is the optical band gap and n is a constant associated to the different types of electronic transitions (n = ½ for direct allowed, $n = 2$ for indirect allowed, $n = 3/2$ for direct forbidden and $n = 3$ for indirect forbidden). E_{gap} values were measured considering a direct allowed electronic transition in equation (3) and the values were evaluated by the extrapolation of the linear portion of the curve considering linear regression of r = 0,99. For $Ca_{1-x}Mg_xTiO_3$ powders (Fig. 3(a)) were founded a E_{gap} values of 3.51 ($x = 0.000$), 2.96 ($x = 0.005$), 2.89 ($x = 0.01$) and 3.44 ($x = 0.02$), respectively.

The calculated band structures [35,34,33,41] show that the electronic transition for $CaTiO_3$ powders occurs inside $[TiO_6]$ octahedral clusters since 2*p* orbitals of oxygen atoms in valence band and 3*d* orbitals of the titanium atoms can be associated with the conduction band. These electronic states are located in the same Brillouin region. However, for $Ca_{1-x}Mg_xTiO_3$ powders 3s orbitals states of Mg atoms will be associated to the conduction band [42,43], so a decrease of the optical gap is observed.

The different band gap values indicate the existence of various intermediary levels between the CB and VB, which is affected by Mg^{2+} concentration in the A-site of $CaTiO_3$. This factor can favor or inhibit the formation of structural defects, which are able to control the degree of structural order–disorder of the material and consequently, the number of intermediary energy levels within band gap [44]. Thus, decrease in the bandgap can be attributed to defects, such as distortions along Ca–O linkages which yield localized electronic levels in the band gap. Moreover, the presence of TiO_2 secondary phase can be responsible for the conductive character observed for $Ca_{1-x}Mg_xTiO_3$ powders with $x = 0.005$ and $x = 0.01$ of Mg^{2+} ions.

$Ca_{1-x}Mg_{x/2}Eu_{2y/3}TiO_3$ powders with $x = 0.001$, 0.002, 0.003 and 0.004 presented E_{gap} values of 3.51 eV, 3.55 eV, 3.52 eV and 3.66 eV, respectively. In the $Ca_{1-x}Mg_yEu_zTiO_3$ powders, when the concentration of Mg^{2+} and Eu^{3+} increases from 0.000 to 0.003, E_{gap} values are practically constant. Absorbance measurements for these samples suggests that the density of localized states in the band gap did not change as Mg^{2+} and Eu^{3+} ions were added to the $CaTiO_3$ matrix. The $x = 0.004$ powder presented an increase in the E_{gap} when compared to the other samples. This behavior can be associated to the formation of a solid solution, being in accordance to the Rietveld refinement analysis.

3.4. Photoluminescence measurements

Since Canham et al. [45] studies, the PL spectroscopy has been the objective of several studies and it is considered a powerful technique to understand the carrier recombination and quantitative characterization of crystals and heterointerfaces [36]. The proposed model by Anicete-Santos et al. [46] considered photoluminescent emission recurrent from radiative recombination of (h•)–electron (e^-)-polarons in the existing energy levels between BV and BC, which is associated with the presence of imperfections or defects in the crystal lattice. To evaluate the effect of Mg doping in $Ca_{1-x}Mg_xTiO_3$ prepared by the PPM, the photoluminescence response for all powders was studied under excitation centered in the host matrix ($\lambda = 350$ nm, room temperature).

PL emission of $Ca_{1-x}Mg_xTiO_3$ powders (Fig.4(a)) covers the visible and infrared region of the electromagnetic spectrum. Three broad bands emissions are observed: one situate at 445 nm (blue region) associated to $CaTiO_3$ matrix, a broad band at 625 nm (red region) ascribed to $MgTiO_3$ [47] phase and a broad band at 800 nm (infrared region) associated to the presence of rutile TiO_2 [48].

The obtained results showed that all these systems presented a PL emission band characteristic of a multiphotonic process, i.e., a system in which relaxation occurs by several paths involving the participation of numerous states within the bandgap of the material. Thus, the decomposition of these broad bands can be used to get the information of which electronic transitions group is influencing the PL response (Fig. 5). The decomposition of the $CaTiO_3$ emission band was performed using the deconvolution method by PeakFit [49] Program (version 4.05). The Gaussian function was successfully used to fit the PL peaks and tuning parameters, including the peak positions and its corresponding areas.

From deconvolution method, it was verified that the PL emission of $Ca_{1-x}Mg_xTiO_3$ powders are composed by three components; a violet component with a maximum situated at around 420 nm, a blue component with a maximum at around 450 nm and the green component with a maximum at 505 nm. Besides that, PL curves is centered at the blue region of the electromagnetic spectrum, and $Ca_{1-x}Mg_xTiO_3$ (x = 0.01) powder presented the highest percentage (74.5%). This observation confirmed that the PL response is directly ascribed to localized states in the band gap due to structural defects in the $Ca_{1-x}Mg_xTiO_3$ crystalline structure. The blue emission (more energetic) indicates the redistribution of energetic states, which is related to the insert of deep defects between conduction and valence bands.

MR and Rietveld analyses showed that the introduction of Mg^{2+}

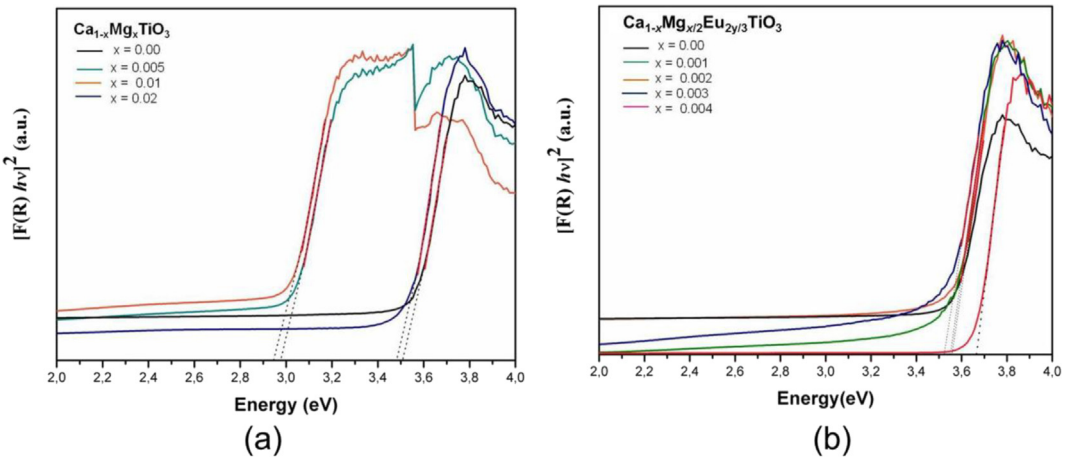

Fig. 3. UV–vis absorption spectra of $Ca_{1-x}Mg_xTiO_3$ (a) and $Ca_{1x}Mg_{x/2}Eu_{2y/3}TiO_3$ (b) powders prepared by the polymeric precursor method.

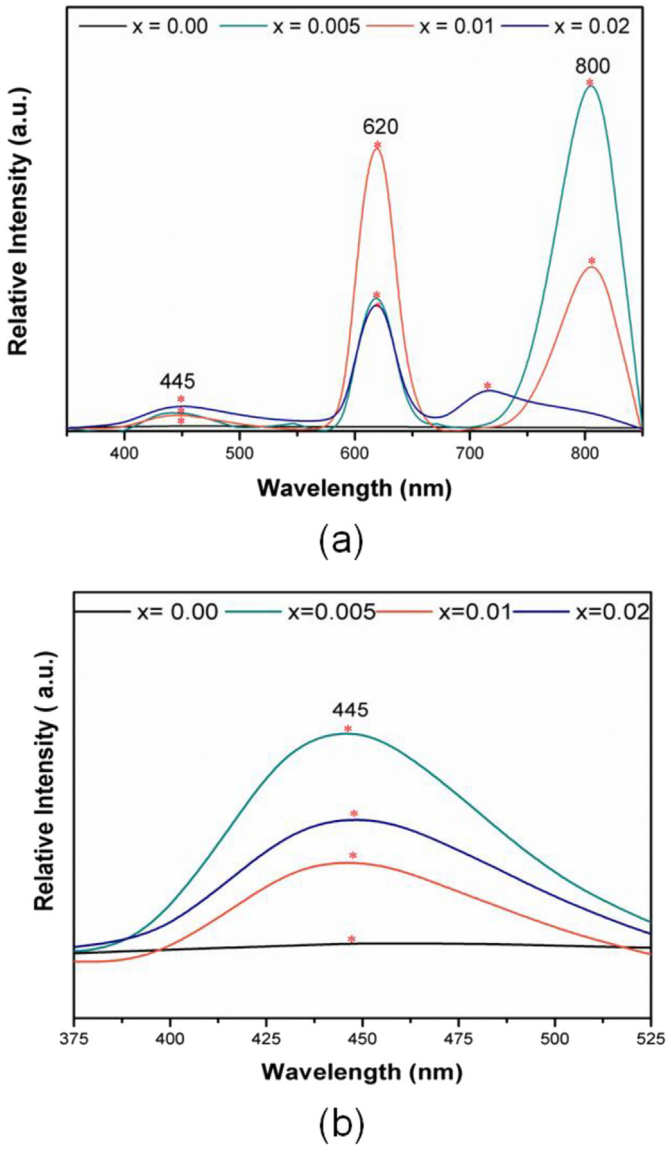

Fig. 4. PL spectra of $Ca_{1-x}Mg_xTiO_3$ powders with $x = 0.000$, 0.005, 0.01 and 0.02 mol of Mg^{2+} ions with an excitation wavelength of 350 nm centered in $CaTiO_3$ matrix.

ions in the A-site of $CaTiO_3$ induced the symmetry break in $[CaO_{12}]$ clusters corroborating to modifications in charge density along the Ca–O linkages. As a result, distorted $[CaO_{12}]$ clusters ($[CaO_{12}]'_o \leftrightarrow [CaO_{12}]^{\bullet}_d$ (o = ordered, d = desordered)) are formed in the $CaTiO_3$ orthorhombic structure. The presence of these species can increase the number of $[MgO_{12}]'_d$ and $[CaO_{12}]^{\bullet}_d$ complex clusters in $Ca_{1-x}Mg_xTiO_3$ powders. Also, these kinds of clusters cause the formation of intermediary levels within band gap. The electronic transitions between $[MgO_{12}]'_d$ and $[CaO_{12}]^{\bullet}_d$ states can be classified as charge transference processes, and the PL response is an indication that the number of these energy levels within the band gap is enhanced by Mg^{2+} doping. Therefore, photoluminescence response can be a result from charge transference from $[CaO_{12}]^{\bullet}_d$ to $[MgO_{12}]'_d$ species in $Ca_{1-x}Mg_xTiO_3$ powders. This phenomenon can be represented by the Kroger-Vink [50] notation at equation (4) below:

$$[CaO_{12}]^{x}_{o} + [CaO_{12}]^{X}_{d} \rightarrow [CaO_{12}]'_{o} + [CaO_{12}]^{\bullet}_{d} \quad (4)$$

$$[MgO_{12}]^{x}_{o} + [CaO_{12}]'_{O} \rightarrow [MgO_{12}]'_{d} + [CaO_{12}]^{\bullet}_{d}$$

Eu^{3+} ions is one of the most interesting ions to study site selection spectroscopy technique because of its optical properties are very sensitive to its local environment. The intensity and splitting of the spectral lines provide useful information concerning the local site symmetry, size of cations and properties of chemical bonds [51].

The monitoring of Eu^{3+} optical properties as function of concentration in $Ca_{1x}Mg_{x/2}Eu_{2y/3}TiO_3$ powders is very important for understanding the nature of lattice modifiers as well as the order-disorder degree in orthorhombic structure. Thus, PL response of $Ca_{1x}Mg_{x/2}Eu_{2y/3}TiO_3$ powders were performed by the emission and excitation spectra centered on the *4f-4f* Eu^{3+} transitions and the obtained results are discussed above.

Fig. 6 shows excitation spectra of the $Ca_{1x}Mg_{x/2}Eu_{2y/3}TiO_3$ powders monitored under emission wavelength of 617 nm at room temperature. In the 350–550 nm spectral range, some narrow bands are visualized due to electronic transitions from the ground $^7F_0$ fundamental state to the excited $^5G_6$ one at 362 nm, $^5H_4$ at 376 nm, $^5L_6$ at 397 nm, $^5D_2$ at 465 nm and $^5D_1$ at 533 nm states [52]. The main electronic transition is assigned to the $^7F_0$ fundamental state to the $^5L_6$ excited state at 397 nm. Below 350 nm none broad band attributed to the cluster–cluster charge transference was observed.

Fig. 7 presents the emission spectra of $Ca_{1-x}Mg_{x/2}Eu_{2y/3}TiO_3$

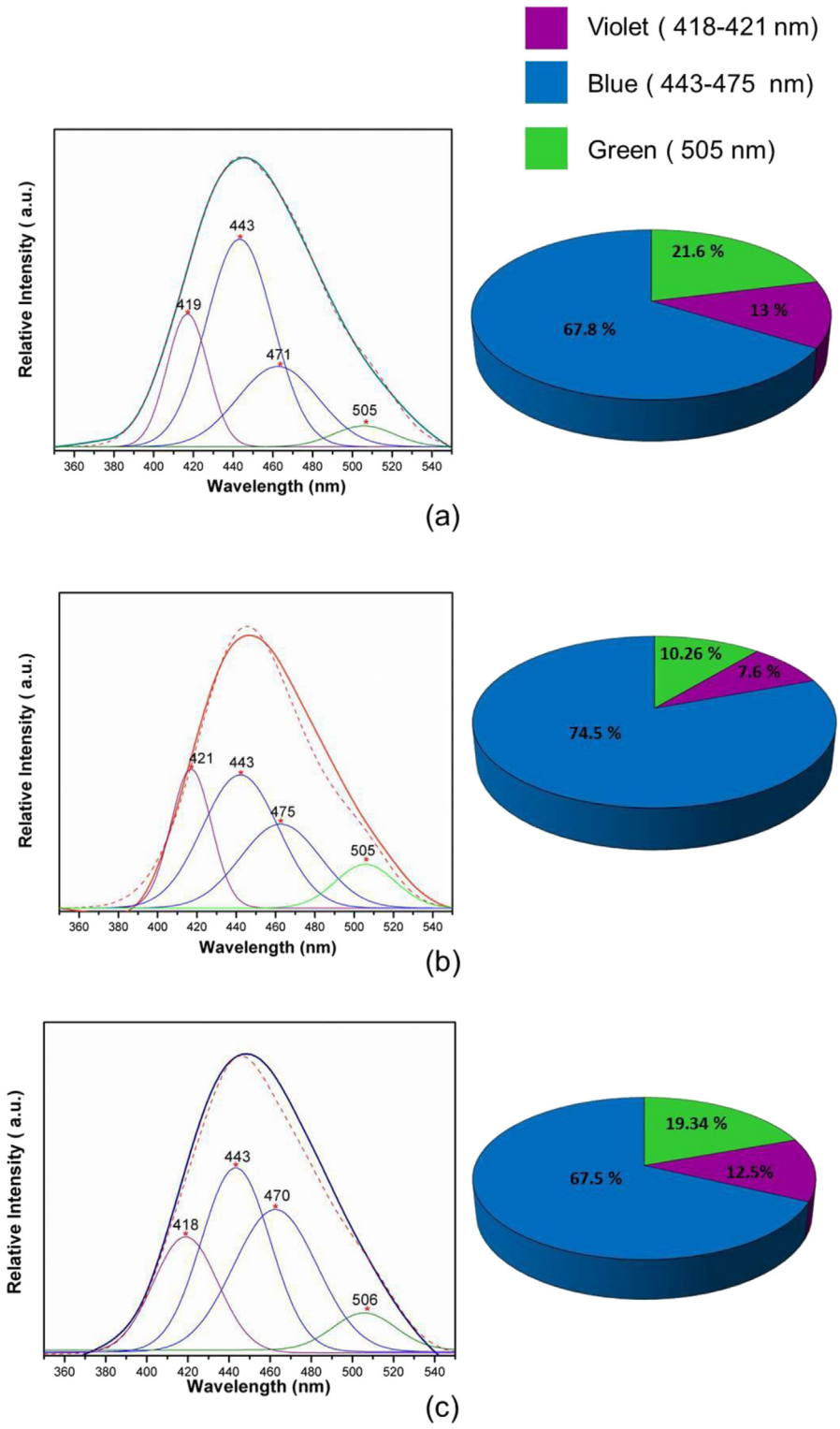

Fig. 5. Decomposition of PL emission spectra of $Ca_{1-x}Mg_xTiO_3$ powders with $x = 0.005$ (a), 0.01(b) and 0.02 (c) mol of Mg^{2+} ions, respectively.

powders with $x = 0.001$, 0.002, 0.003 and 0.004 of Mg^{2+} and Eu^{3+} ions monitored under excitation wavelength of 397 nm. During the emission process all the electrons in excited $^5D_0$ state, returns to the ground states by the radiative decay process. This energy is emitted in the visible range of electromagnetic spectrum. The group of emission lines at 583, 592, 617, 656 and 697 nm are assigned to the emission transitions from $^5D_0$ excited states to the ^7F_J (J = 0, 1, 2, 3 and 4) ground states, respectively [11,53].

Analyzing these emission spectra, the $^5D_0 \rightarrow {}^7F_1$ transition at 583 nm is composed by three Stark components. Moreover, $^5D_0 \rightarrow {}^7F_2$ transition at 617 nm is the most intense band in all emission spectra indicating that ligand field strongly perturbs the Eu^{3+} ions [54]. The relative intensity of these bands did not modify with the concentration of Eu^{3+} ions.

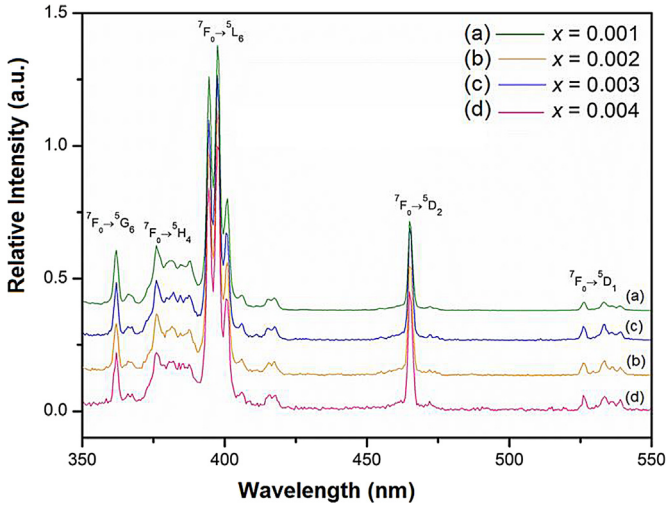

Fig. 6. Excitation spectra of $Ca_{1x}Mg_{x/2}Eu_{2y/3}TiO_3$ powders with $x = 0.001$ (a), 0.002 (b), 0.003(c) and 0.004 (d) obtained using an emission wavelength of 617 nm, at room temperature.

The intensity of the $^5D_0 \rightarrow {}^7F_2$ transition can be changed by chemical interaction around the rare earth ion, while the magnetic dipole $^5D_0 \rightarrow {}^7F_1$ transition at 590 nm, is independent of the crystalline field [55]. Considering the ratio between the intensities of these two transitions, the local symmetry of Eu^{3+} sites can be measured and the larger value of this ratio can be associated to a more distortion degree from the inversion symmetry [56].

In this work, $^5D_0 \rightarrow {}^7F_2$ (A_{02})/$^5D_0 \rightarrow {}^7F_1$ (A_{01}) ratio was measured and the correspondent 2.18, 1.75, 2.16 and 2.73 values were obtained for the $Ca_{1x}Mg_{x/2}Eu_{2y/3}TiO_3$ powders with $x = 0.001$; 0.002; 0.003 and 0.004, respectively. These results showed that Eu^{3+} ions are located at low symmetry sites, i.e., Eu^{3+} ions are located in a distorted or asymmetric cation environment in $CaTiO_3$ matrix. Therefore, we believe that distorted cation environment around Eu^{3+} ions can be attributed to double ionized calcium vacancies in the A-site of $CaTiO_3$ crystalline structure. For $Ca_{1-x}Mg_xTiO_3$ powders, the PL emission can be mainly attributed to charge transference between $[CaO_{12}]^{\bullet}_d \rightarrow [MgO_{12}]^{'}_d$ clusters. Thus, we

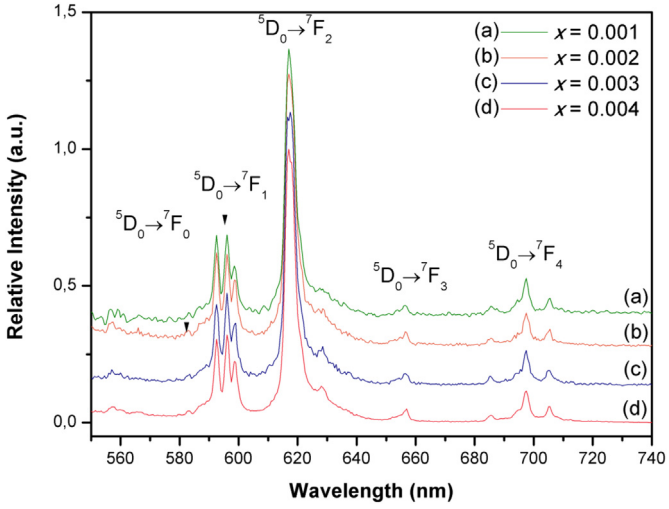

Fig. 7. Emission spectra of $Ca_{1x}Mg_{x/2}Eu_{2y/3}TiO_3$ powders with $x = 0.001$ (a), 0.002 (b), 0.003 (c) and 0.004 (d) mol of Mg^{2+} and Eu^{3+} ions obtained using an excitation wavelength of 397 nm, at room temperature.

believe that Mg^{2+} ions in the $Ca_{1x}Mg_{x/2}Eu_{2y/3}TiO_3$ powders can increase the number of $[MgO_{12}]^{'}_d$ clusters in these systems. As a consequence, there is a formation of mono-ionized calcium vacancies in $CaTiO_3$ matrix. Based on this hypothesis, the $Ca_{1x}Mg_{x/2}Eu_{2y/3}TiO_3$ improved luminescence response is due to the presence of $[V^{'}_{Ca}O_{12}]$ as well as $[V^{''}_{Ca}O_{12}]$ species in $CaTiO_3$ structure. The charge compensation are represented by the Kroger-Vink [50] notation at equation (5) below

$$2[EuO_{12}]^x + \left[V^x_{Ca}O_{12}\right] \rightarrow 2[EuO_{12}]^{\bullet} + \left[V^{''}_{Ca}O_{12}\right]$$

$$\left[V^x_{Ca}O_{12}\right] + [MgO_{12}]^{'} \rightarrow \left[V^{'}_{Ca}O_{12}\right] + [MgO_{12}]^x \quad (5)$$

$Ca_{1x}Mg_{x/2}Eu_{2y/3}TiO_3$ decay curves of Eu^{3+} $^5D_0 \rightarrow {}^7F_2$ transition (not shown), presented a mono-exponential feature when this ion when the excitation and emission wavelength was set at 397 and 617 nm, respectively. As the Mg/Eu increases, the lifetime values enhanced for $0.000 < x < 0.002$ systems. However, $x = 0.003$ system presented the highest lifetime indicating that the best concentration of Mg^{2+} and Eu^{3+} in $CaTiO_3$ was 0.3% mol. On the other hand, the $x = 0.004$ system presented a decrease in the lifetime value. In this system, the Eu^{3+} emission quenching can be attributed to high concentration of Eu^{3+} in this system. With increasing the Eu^{3+} concentration, the distance between Eu^{3+} ions become closer, and thus the probability of energy transfer between these species is higher [57].

4. Conclusions

In summary, $Ca_{1-x}Mg_xTiO_3$ and $Ca_{1x}Mg_{x/2}Eu_{2y/3}TiO_3$ powders were prepared by the polymeric precursor method. Rietveld and MR analyses confirmed the substitution of Ca^{2+} by Mg^{2+} and Ca^{2+} by Mg^{2+} and Eu^{3+} ions in the A site of $CaTiO_3$ matrix. Such substitutions were associated to structural defects such as distortions and/or calcium vacancies into its crystalline structure. Photoluminescence study showed that the $Ca_{1-x}Mg_xTiO_3$ powders presented a broad emission band centered at 450 nm (blue region) and the PL response was associated to symmetry break in $[CaO_{12}]$ clusters corroborating to modifications in charge density along the Ca–O linkages. Excitation, emission and decay curves of $Ca_{1x}Mg_{x/2}Eu_{2y/3}TiO_3$ powders were also studied. The emission spectra presented the Eu^{3+} characteristic $^5D_0 \rightarrow {}^7F_J$ (J = 0, 1, 2, 3 and 4) electronic transition sharp bands. The calculus of the relative area (A_{02}/A_{01}) of $^5D_0 \rightarrow {}^7F_2$ (A_{02}) and $^5D_0 \rightarrow {}^7F_1$ (A_{01}) 4f transitions of Eu^{3+} ions indicated the presence of Eu^{3+} ions in low symmetry sites. The Eu^{3+} in the A-site of $CaTiO_3$ crystalline structure induced the formation of double ionized calcium vacancies. Moreover, the luminescence data showed that Mg^{2+} and Eu^{3+} co-doping increased the concentration of calcium vacancies into $CaTiO_3$ matrix, improving its optical properties.

Acknowledgments

The authors appreciate the support of the following Brazilian research financing institutions CAPES, CNPq and FAPESP.

References

[1] A. Boudali, A. Abada, M. Driss Khodja, B. Amrani, K. Amara, F. Driss Khodja, et al., Calculation of structural, elastic, electronic, and thermal properties of orthorhombic $CaTiO_3$, Phys. B Condens. Matter 405 (2010) 3879–3884, http://dx.doi.org/10.1016/j.physb.2010.06.020.

[2] B. Yan, K. Zhou, In situ sol–gel composition of inorganic/organic polymeric hybrid precursors to synthesize red-luminescent $CaTiO_3:Pr^{3+}$ and $CaTi_{0.5}Zr_{0.5}O_3:Pr^{3+}$ phosphors, J. Alloys Compd. 398 (2005) 165–169, http://dx.doi.org/10.1016/j.jallcom.2004.08.109.

[3] B.J. Kennedy, C.J. Howard, B.C. Chakoumakos, Phase transitions in perovskite at elevated temperatures - a powder neutron diffraction study, J. Phys. Condens. Mater. 11 (1999) 1479–1488, http://dx.doi.org/10.1088/0953-8984/11/6/012.

[4] E.A. Nenasheva, L.P. Mudroliubova, N.F. Kartenko, Microwave dielectric properties of ceramics based on $CaTiO_3$–$LnMO_3$ System (Ln–La, Nd; M–Al, Ga), J. Eur. Ceram. Soc. 23 (2003) 2443–2448, http://dx.doi.org/10.1016/S0955-2219(03)00188-2.

[5] E. Cockayne, B.P. Burton, Phonons and static dielectric constant in $CaTiO_3$ from first principles, Phys. Rev. B 62 (2000) 3735–3743, http://dx.doi.org/10.1103/PhysRevB.62.3735.

[6] X.M. Chen, L. Li, X.Q. Liu, Layered complex structures of $MgTiO_3$ and $CaTiO_3$ dielectric ceramics, Mater. Sci. Engeneering B 99 (2003) 255–258, http://dx.doi.org/10.1016/S0921-5107(02)00493-2.

[7] B.D. Lee, H.R. Lee, K.H. Yoon, D.H. Kang, Effect of Stacking layers on the microwave dielectric properties of $MgTiO_3$/$CaTiO_3$ multilayered thin films, J. Am. Ceram. Soc. 88 (2005) 1197–1200, http://dx.doi.org/10.1111/j.1551-2916.2005.00247.x.

[8] H.-K. Shin, H. Shin, S.-T. Bae, S. Lee, K.S. Hong, Effect of oxygen partial pressure during liquid-phase sintering on the dielectric properties of $0.9MgTiO_3$-$0.1CaTiO_3$, J. Am. Ceram. Soc. 91 (2007) 132–138, http://dx.doi.org/10.1111/j.1551-2916.2007.02016.x.

[9] J.Y. Cho, K.H. Yoon, E.S. Kim, Correlation between arrangement of dielectric layers and microwave dielectric properties of $Mg_{0.93}Ca_{0.07}TiO_3$–($Ca_{0.3}Li_{0.14}Sm_{0.42}$)$TiO_3$ ceramics, J. Am. Ceram. Soc. 32 (2003) 1330–1332, http://dx.doi.org/10.1111/j.1151-2916.2003.tb03471.x.

[10] F.C.D. Lemos, D.M.A. Melo, J.E.C. da Silva, Photoluminescence of Er^{3+} doped in $PbTiO_3$ perovskite-type obtained via polymeric precursor method, Opt. Commun. 231 (2004) 251–255, http://dx.doi.org/10.1016/j.optcom.2003.12.035.

[11] W. Sun, Y. Gu, Q. Zhang, Y. Li, H. Wang, $CaTiO_3$:Eu^{3+} layers coated SiO_2 particles: core-shell structured red phosphors for near-UV white LEDs, J. Alloys Compd. 493 (2010) 561–564, http://dx.doi.org/10.1016/j.jallcom.2009.12.155.

[12] P. Boutinaud, E. Tomasella, A. Ennajdaoui, R. Mahiou, Structural characterization and luminescent properties of $CaTiO_3$:Pr^{3+} thin films deposited by radio frequency sputtering, Thin Solid Films 515 (2006) 2316–2321, http://dx.doi.org/10.1016/j.tsf.2006.03.037.

[13] A.T. de Figueiredo, V.M. Longo, S. de Lazaro, V.R. Mastelaro, F.S. De Vicente, A.C. Hernandes, et al., Blue-green and red photoluminescence in $CaTiO_3$:Sm, J. Lumin 126 (2007) 403–407, http://dx.doi.org/10.1016/j.jlumin.2006.08.100.

[14] P.J. Dereń, R. Mahiou, R. Pązik, K. Lemanski, W. Stręk, P. Boutinaud, Upconversion emission in $CaTiO_3$:Er^{3+} nanocrystals, J. Lumin 128 (2008) 797–799, http://dx.doi.org/10.1016/j.jlumin.2007.11.057.

[15] B. Marí, K.C. Singh, P. Cembrero-Coca, I. Singh, D. Singh, S, Chand, Red emitting $MTiO_3$ (M = Ca or Sr) phosphors doped with Eu^{3+} or Pr^{3+} with some cations as co-dopants, Displays 34 (2013) 346–351, http://dx.doi.org/10.1016/j.displa.2013.07.003.

[16] H.K. Yang, J.W. Chung, B.K. Moon, B.C. Choi, J.H. Jeong, K. Jang, et al., Photoluminescence characteristics of Li-doped $CaTiO_3$:Pr^{3+} thin films grown on Si (100) substrate by PLD, Thin Solid Films 518 (2010) 6219–6222, http://dx.doi.org/10.1016/j.tsf.2010.03.171.

[17] G. Gasparotto, S. a. M. Lima, M.R. Davolos, J.A. Varela, E. Longo, M. a. Zaghete, Luminescence properties of Eu^{3+}- and Mg^{2+}-doped $LiTaO_3$ obtained via the polymeric precursor method, J. Lumin 128 (2008) 1606–1610, http://dx.doi.org/10.1016/j.jlumin.2008.03.005.

[18] K. Goto, Y. Nakachi, K. Ueda, Photoluminescence properties of Pr doped and Tb–Mg codoped $CaSnO_3$ with perovskite structure, Thin Solid Films 516 (2008) 5885–5889, http://dx.doi.org/10.1016/j.tsf.2007.10.060.

[19] M.D. Pechini, 1967. Method of Preparing Lead and Alkaline Earth Titanates and Niobates and Coating Method Using the Same to Form a Capacitor, U.S. Pat. No 3,330.697.

[20] S.W. Baertschi, B.W. Pack, C.S. Hoaglund Hyzer, M.A. Nussbaum, Assessing mass balance in pharmaceutical drug products: new insights into an old topic, TrAC Trends Anal. Chem. 49 (2013) 126–136, http://dx.doi.org/10.1016/j.trac.2013.06.006.

[21] D.L. Dorset, X-ray Diffraction: A Practical Approach, Microsc. Microanal. 4 (1998) 513–515, http://dx.doi.org/10.1017/S143192769800049X.

[22] R.B. Larson, A.C. Von Dreele, General Structure Analysis System (GSAS), Los Alamos National Laboratory, 2004. Report No. LAUR, 86.

[23] L.W. Finger, D.E. Cox, A.P. Jephcoat, A correction for powder diffraction peak asymmetry due to axial divergence, J. Appl. Crystallogr. 27 (1994) 892–900, http://dx.doi.org/10.1107/S0021889894004218.

[24] M.M. Mao, X.C. Fan, X.M. Chen, Effect of A-Site Ionic Radius on the Structure and Microwave Dielectric Characteristics of $Sr_{1+x}Sm_{1-x}Al_{1-x}Ti_xO_4$ Ceramics, Int. J. Appl. Ceram. Technol. 7 (2010) E156–E162, http://dx.doi.org/10.1111/j.1744-7402.2010.02492.x.

[25] B.Y.R.D. Shannon, M. H, N.H. Baur, O.H. Gibbs, M. Eu, V. Cu, Revised effective ionic radii and systematic studies of interatomic distances in halides and chalcogenides, Acta Crystallogr. A32 (1976) 751.

[26] P. McMillan, N. Ross, The Raman spectra of several orthorhombic calcium oxide perovskites, Phys. Chem. Min. 16 (1988) 21–28, http://dx.doi.org/10.1007/BF00201326.

[27] U. Balachandran, N.G. Eror, Laser-induced Raman Scattering in Calcium Titanate, Solid State Commun. 44 (1982) 815–818, http://dx.doi.org/10.1107/S0567739476001551.

[28] T. Hirata, K. Ishioka, M. Kitajima, Vibrational spectroscopy and X-ray diffraction of Perovskite compounds $Sr_{1-x}M_xTiO_3$ (M = Ca, Mg; $0 \geq x \geq 1$), J. Solid State Chem. 124 (1996) 353–359, http://dx.doi.org/10.1006/jssc.1996.0249.

[29] H. Zheng, I.M. Reaney, G.D.C.C. de Györgyfalva, R. Ubic, J. Yarwood, M.P. Seabra, et al., Raman spectroscopy of $CaTiO_3$-based perovskite solid solutions, J. Mater. Res. 19 (2004) 488–495, http://dx.doi.org/10.1557/jmr.2004.19.2.488.

[30] Y. Li, S. Qin, F. Seifert, Phase transitions in A-site substituted perovskite compounds: the ($Ca_{1-2x}Na_xLa_x$)TiO_3 ($0 \leq x \leq 0.5$) solid solution, J. Solid State Chem. 180 (2007) 824–833, http://dx.doi.org/10.1016/j.jssc.2006.12.012.

[31] L.H. Oliveira, A.P. de Moura, T.M. Mazzo, M.A. Ramírez, L.S. Cavalcante, S.G. Antonio, et al., Structural refinement and photoluminescence properties of irregular cube-like ($Ca_{1-x}Cu_x$)TiO_3 microcrystals synthesized by the microwave–hydrothermal method, Mater. Chem. Phys. 136 (2012) 130–139, http://dx.doi.org/10.1016/j.matchemphys.2012.06.042.

[32] Y. Hanajiri, T. Matsui, Y. Arita, T. Nagasaki, H. Shigematsu, T. Harami, EXAFS analyses of $CaTiO_3$ doped with Ce, Nd and U, Solid State Ionics 108 (1998) 343–348, http://dx.doi.org/10.1016/S0167-2738(98)00061-7.

[33] J. Milanez, A.T. de Figueiredo, S. de Lazaro, V.M. Longo, R. Erlo, V.R. Mastelaro, et al., The role of oxygen vacancy in the photoluminescence property at room temperature of the $CaTiO_3$,, J. Appl. Phys. 106 (2009) 043526, http://dx.doi.org/10.1063/1.3190524.

[34] S. De Lazaro, J. Milanez, A.T. De Figueiredo, V.M. Longo, V.R. Mastelaro, F.S. De Vicente, et al., Relation between photoluminescence emission and local order-disorder in the $CaTiO_3$ lattice modifier, Appl. Phys. Lett. 90 (2007) 10–12, http://dx.doi.org/10.1063/1.2713359.

[35] M.L. Moreira, E.C. Paris, G.S. do Nascimento, V.M. Longo, J.R. Sambrano, V.R. Mastelaro, et al., Structural and optical properties of $CaTiO_3$ perovskite-based materials obtained by microwave-assisted hydrothermal synthesis: an experimental and theoretical insight, Acta Mater. 57 (2009) 5174–5185, http://dx.doi.org/10.1016/j.actamat.2009.07.019.

[36] Y. Wu, Z. Sun, K. Ruan, Y. Xu, H. Zhang, Enhancing photoluminescence with Li-doped $CaTiO_3$:Eu^{3+} red phosphors prepared by solid state synthesis, J. Lumin 155 (2014) 269–274, http://dx.doi.org/10.1016/j.jlumin.2014.06.051.

[37] J. Tang, X. Yu, L. Yang, C. Zhou, X. Peng, Preparation and Al^{3+} enhanced photoluminescence properties of $CaTiO_3$:Pr^{3+}, Mater. Lett. 60 (2006) 326–329, http://dx.doi.org/10.1016/j.matlet.2005.08.047.

[38] W. Yang, J. Hu, Synthesis and luminescence properties of hexagonal $CaTiO_3$:Eu^{3+} nanosheets, J. Lumin 145 (2014) 144–147, http://dx.doi.org/10.1016/j.jlumin.2013.07.041.

[39] T.M. Mazzo, I.M. Pinatti, L.R. Macario, W. Avansi, M.L. Moreira, I.L.V. Rosa, et al., Europium-doped calcium titanate: optical and structural evaluations, J. Alloys Compd. 585 (2014) 154–162, http://dx.doi.org/10.1016/j.jallcom.2013.08.174.

[40] P. Kubelka, F. Munk, Ein beitrag zur optik der farbanstriche, Tech. Phys. 12 (1931) 593–601.

[41] F.M. Pontes, C.D. Pinheiro, E. Longo, E.R. Leite, S.R. De Lazaro, J.A. Varela, et al., The role of network modifiers in the creation of photoluminescence in $CaTiO_3$, Mater. Chem. Phys. 78 (2003) 227–233, http://dx.doi.org/10.1016/S0254-0584(02)00230-4.

[42] T. Mizoguchi, M. Yoshiya, J. Li, F. Oba, I. Tanaka, H. Adachi, Electron-energy-loss near edge structures of six-fold-coordinated Zn in MgO, Ultramicroscopy 86 (2001) 363–370, http://dx.doi.org/10.1016/S0304-3991(00)00127-3.

[43] X. Qiu, L. Li, J. Zheng, J. Liu, X. Sun, G. Li, Origin of the enhanced photocatalytic activities of semiconductors: a case study of ZnO doped with Mg^{2+}, J. Phys. Chem. C 112 (2008) 12242–12248, http://dx.doi.org/10.1021/jp803129e.

[44] M.A.P. Almeida, L.S. Cavalcante, J.A. Varela, M. Siu Li, E. Longo, Effect of different surfactants on the shape, growth and photoluminescence behavior of $MnWO_4$ crystals synthesized by the microwave-hydrothermal method, Adv. Powder Technol. 23 (2012) 124–128, http://dx.doi.org/10.1016/j.apt.2011.10.004.

[45] L.T. Canham, Silicon quantum wire array fabrication by electrochemical and chemical dissolution of wafers, Appl. Phys. Lett. 57 (1990) 1046, http://dx.doi.org/10.1063/1.103561.

[46] M. Anicete-Santos, E. Orhan, M.A.M.A. De Maurera, L.G.P. Simões, A.G. Souza, P.S. Pizani, et al., Contribution of structural order-disorder to the green photoluminescence of $PbWO_4$, Phys. Rev. B Condens. Matter Mater. Phys. 75 (2007) 1–11, http://dx.doi.org/10.1103/PhysRevB.75.165105.

[47] E.A.V. Ferri, J.C. Sczancoski, L.S. Cavalcante, E.C. Paris, J.W.M. Espinosa, A.T. de Figueiredo, et al., Photoluminescence behavior in $MgTiO_3$ powders with vacancy/distorted clusters and octahedral tilting, Mater. Chem. Phys. 117 (2009) 192–198, http://dx.doi.org/10.1016/j.matchemphys.2009.05.042.

[48] J. Shi, J. Chen, Z. Feng, T. Chen, Y. Lian, X. Wang, et al., Photoluminescence characteristics of TiO_2 and their relationship to the photoassisted reaction of water/methanol mixture, J. Phys. Chem. C 111 (2007) 693–699, http://dx.doi.org/10.1021/jp065744z.

[49] PEAKFIT, SeaSolve Software Inc 4.12.

[50] F.A. Kroger, H.J. Vink, Relations between the concentrations of imperfections in solids, J. Phys. Chem. Solids 5 (1958) 208–223, http://dx.doi.org/10.1016/0022-3697(58)90069-6.

[51] P.F.S. Pereira, A.P. de Moura, I.C. Nogueira, M.V.S. Lima, E. Longo, P.C. de Sousa Filho, O.A. Serra, E.J. Nassar, I.L.V. Rosa, Study of the annealing temperature effect on the structural and luminescence properties of $SrWO_4$:Eu phosphors prepared by a non-hydrolitic sol-gel process, J. Alloys Compd. 526 (2012) 11–21.

[52] E.E. Teotonio, M.C.F. Felinto, H.F. Brito, O.L. Malta, A.C. Trindade, R. Najjar, et al., Synthesis, crystalline structure and photoluminescence investigations of the new trivalent rare earth complexes (Sm^{3+}, Eu^{3+} and Tb^{3+}) containing 2-thiophenecarboxylate as sensitizer, Inorganica Chim. Acta 357 (2004) 451–460, http://dx.doi.org/10.1016/j.ica.2003.08.009.

[53] D.T.M. Huong, N.H. Nam, L. Van Vu, N.N. Long, Preparation and optical characterization of Eu^{3+}-doped $CaTiO_3$ perovskite powders, J. Alloys Compd. 537 (2012) 54–59, http://dx.doi.org/10.1016/j.jallcom.2012.05.087.

[54] H. Liang, F. Xie, Luminescence of a conjugated polymer containing europium (III) chelate, J. Lumin. 144 (2013) 230–233, http://dx.doi.org/10.1016/j.jlumin.2013.08.014.

[55] I.L.V. Rosa, L.H. Oliveira, C.K. Suzuki, J. a Varela, E.R. Leite, E. Longo, SiO_2-GeO_2 soot preform as a core for Eu_2O_3 nanocoating: synthesis and photophysical study, J. Fluoresc. 18 (2008) 541–545, http://dx.doi.org/10.1007/s10895-007-0297-7.

[56] M.G. Ha, J.H. Lee, J.S. Bae, J.P. Kim, K.S. Hong, H.-S. Yang, Photophysical properties of highly efficient red-emitting $CaTiO_3$:Eu^{3+} phosphors under near ultra-violet excitation, Curr. Appl. Phys. 11 (2011) 1379–1383, http://dx.doi.org/10.1016/j.cap.2011.04.008.

[57] M. Shivram, S.C. Prashantha, H. Nagabhushana, S.C. Sharma, K. Thyagarajan, R. Harikrishna, et al., $CaTiO_3$:Eu^{3+} red nanophosphor: low temperature synthesis and photoluminescence properties. Spectrochim. Acta. A. Mol. Biomol. Spectrosc. 120 (2014) 395–400, http://dx.doi.org/10.1016/j.saa.2013.09.114.